International Journal of Heat and Mass Transfer 153 (2020) 119657

Contents lists available at ScienceDirect

International Journal of Heat and Mass Transfer

journal homepage: www.elsevier.com/locate/hmt

A pore-scale assessment of the dynamic response of forced convection in porous media to inlet flow modulations

Rabeeah Habib[a], Nader Karimi[a,b,*], Bijan Yadollahi[a], Mohammad Hossein Doranehgard[c], Larry K.B. Li[d]

[a] James Watt School of Engineering, University of Glasgow, Glasgow G12 8QQ, United Kingdom
[b] School of Engineering and Materials Science, Queen Mary University of London, London E1 4NS, United Kingdom
[c] Department of Civil and Environmental Engineering, School of Mining and Petroleum Engineering, University of Alberta, Edmonton, Alberta, T6G 1H9, Canada
[d] Department of Mechanical and Aerospace Engineering, Hong Kong University of Science and Technology, Clear Water Bay, Kowloon, Hong Kong

ARTICLE INFO

Article history:
Received 23 December 2019
Revised 7 March 2020
Accepted 12 March 2020

Keywords:
Pore-scale analysis
Porous media
Dynamic response
Unsteady forced convection
Transfer function
Nonlinear response

ABSTRACT

An increasing number of technologies require prediction of unsteady forced convection in porous media when the inlet flow is unsteady. To gain further insight into this problem, the unsteady equations of continuity, Navier Stokes and energy are solved within the pores formed by several cylindrical flow obstacles. The system is modulated by sine waves superimposed on the inlet flow velocity, and the spatio-temporal responses of the flow and temperature fields are calculated. The results are then utilised to assess the linearity of the thermal response represented by the Nusselt number on the obstacles. It is shown that for linear cases, a transfer function can be devised for predicting the dynamic response of the Nusselt number. It is further argued that such a transfer function can be approximated by a classic low-pass filter which resembles the average response of the individual obstacles. This indicates that there exists a frequency threshold above which the thermal system is essentially insensitive to flow modulations. The results also show that changes in Reynolds number and porosity of the medium can push the dynamic response of the system towards non-linearity. Yet, there appears to be no monotonic change in the linearity of the response with respect to the Reynolds number and porosity. In general, it is found that for low Reynolds numbers, the dynamics of heat convection can be predicted decently by taking a transfer function approach. The findings of this study can enable further understanding of unsteady forced convection in porous media subject to time-varying inlet flows.

© 2020 The Authors. Published by Elsevier Ltd.
This is an open access article under the CC BY license. (http://creativecommons.org/licenses/by/4.0/)

1. Introduction

The use of porous media in emerging technologies [1,2,3,4,5], including electrochemical systems [6,7] combustion of carbon-neutral and renewable fuels [8,9], and micro chemical reactors [10,11], requires an understating of their dynamic responses. This is because in these applications the inlet fluid flow rate can become strongly time dependant [12]. Furthermore, it is essential to be able to predict the thermal response of the system to temporal disturbances superimposed on the inlet flow [13]. Yet, existing investigations of forced convection in porous media have focused largely on steady phenomena. This trend could be readily observed in studies involving macroscopic modelling (e.g. [14,15,16,17,18]) as well as in those taking a pore-scale approach to the analysis of heat convection in porous media (e.g. [19,20,21,22,23,24,25]).

Over the last two decades, most theoretical and numerical studies on porous media have been based on the Darcy model and its extensions [26,27,28,29,30]. Nevertheless, it has been implied that the application of this model to periodic flow systems is not straightforward [6] and thus a pore-scale approach is sometimes used for greater accuracy. A small number of studies have investigated unsteady and oscillatory flows in porous media in two-dimensional domains [7,8,9,10], and even fewer studies have examined three-dimensional domains [11]. As a result, there appears to be a gap in understanding the dynamic response of heat transfer in porous media to time-varying flows. To evaluate the status of steady and unsteady pore-scale modelling, here a concise review of the literature on microscopic studies in porous media is put forward.

* Corresponding author.
E-mail address: nader.karimi@glasgow.ac.uk (N. Karimi).

https://doi.org/10.1016/j.ijheatmasstransfer.2020.119657
0017-9310/© 2020 The Authors. Published by Elsevier Ltd. This is an open access article under the CC BY license. (http://creativecommons.org/licenses/by/4.0/)

Nomenclature

List of symbols

a	amplitude $= (max.sin(2\pi \cdot f \cdot t) - min.sin(2\pi \cdot f \cdot t))/2$
c_p	specific heat capacity (J K^{-1} kg^{-1})
C	capacitance (F)
d	obstacle distance from the inlet (m)
D	particle diameter (m)
f	frequency (Hz)
h_o	external heat convection coefficient (W m^{-2} K^{-1})
H	height (m)
k	thermal conductivity (W K^{-1} m^{-1})
l	length (m)
$\dot{m}$	mass flow rate (kg s^{-1})
n	Euclidean distance of the normalized Nusselt number at each particle
Nu	Nusselt number (-)
o	Discrete Fourier transform single sided amplitude spectrum of the normalized Nusselt number at each particle
p	pressure (Pa)
q''	heat flux (W m^{-2})
R	resistance (Ω)
Re	Reynolds number (-)
St	$(f \cdot D)/u$
t	time (s)
T	temperature (K)
u	flow velocity (m s^{-1})
X_C	capacitive reactance (Ω)

Greek symbols

μ	dynamic viscosity
ε	porosity
ρ	density
ϕ	phase
ω	angular frequency
δ	measure of non-linearity
ψ	temperature/velocity

Subscripts

amb	ambient
delay	delay
c	cut-off
D	based on Darcy
f	fluid
i	obstacle number
in	inlet
L	based on particle diameter size
ref	reference
x, y, z	cartesian coordinates

Superscript

$\bar{}$	mean

Inspired by the macroscopic study of Kuwahara et al. [31], Gamrat et al. [23] numerically investigated heat transfer over banks of square rods in aligned and staggered arrangements with a varying porosity between 0.44 and 0.98. The two-dimensional laminar flow model focussed on low Reynolds number flows and with two thermal boundary conditions: constant wall temperature and constant volumetric heat source. The effects of bank arrangements, porosity, Prandtl and Reynolds number upon the value of the Nusselt number were examined. Gamrat et al. [23] showed that the convective heat transfer coefficient obtained with a constant wall temperature was significantly higher than previously reported results. In a similar context, Teruel and Diaz [32] simulated a microscopic laminar flow developed through a porous medium formed by staggered square cylinders. They modelled multiple representative elementary volumes (REV) to validate their calculations of macroscopic parameters, such as the interfacial heat transfer coefficient by employing a unit periodic cell. The steady flow regime was varied with Peclet numbers in the range of 10–1000 and porosities between 0.55–0.95. The interfacial heat transfer coefficient was also calculated as a function of the REV positions in the porous structure showing position dependency or pore-scale fluctuations.

Two-dimensional square and circular cross-sectional models in a staggered arrangement were developed by Torabi et al. [20]. A steady laminar flow was numerically simulated with a constant inlet temperature and solid phase temperature. These authors [20] performed a thermodynamic analysis of forced convection through porous media with a particular focus on entropy generation. A range of Reynolds numbers and porosities were considered for both Darcy and Forchheimer flow regimes. In keeping with the findings of macroscopic models, the results showed that increasing the Reynolds number or decreasing the porosity of the medium enhances the rate of heat transfer.

Ozgumus and Mobedi [21] examined the effects of the pore-to-throat size ratio on the interfacial heat transfer coefficient for a periodic, two-dimensional porous media containing an inline array of rectangular rods. The velocity and temperature distributions in the voids between the rods were calculated numerically for the REV using the Navier Stokes equations. The effects of variations in the pertinent parameters including porosity, the Reynolds number and the pore-to-throat size ratio were considered. Ozgumus and Mobedi [21] found that the pore-to-throat size ratio could considerably affect the interfacial convective heat transfer coefficient. According to their results, an increase in porosity increases the Nusselt number for low pore-to-throat size ratios, but it decreases the Nusselt number for high pore-to-throat size ratios.

In an attempt to gain further insight into combustion in porous media, Jouybari et al. [33] conducted a pore-scale simulation of turbulent reacting flow of air/methane mixture. This study was mainly concerned with the investigation of multi-dimensional effects and turbulence on the flame within the pores of a reticulated porous medium. The investigated two-dimensional medium consisted of a staggered arrangement of square cylinders, similar to that of Teruel and Diaz [32]. The stationary Reynolds averaged Navier-Stokes, energy conservation, the species conservation, and a turbulence model were solved using a finite volume technique. In this study, the turbulence kinetic energy, turbulent viscosity ratio, temperature, flame speed, convective heat transfer, and thermal conductivity were compared for laminar and turbulent simulations. Jouybari et al. [33] showed that unlike the previous volume-averaged simulations (macroscopic) which predicted a flat flame in the porous medium, a highly curved flame anchored to the square cylinders was detected in their study.

Wu et al. [34] numerically simulated convective heat transfer between air flow and ceramic foams to optimise the volumetric solar air receiver performances. They computed the local convective heat transfer coefficient between the air flow and ceramic porous foam for which the flow momentum and energy balance were solved inside the porous ceramic foam. A sensitivity study on the heat transfer coefficient was conducted with the porosity, velocity and mean cell size parameters. The Reynolds number based on the pore diameter was between 240–1600, where part of the flow regime was laminar and the solid was kept at a uniform temperature. Wu et al. [34] stated that the difference between the laminar flow and the turbulence model was insignificant and therefore their study considered only a turbulent flow. The inlet temperature was kept smaller than the constant temperature of the ceramic foam to study the convective heat transfer coefficient

values. The flow field and heat transfer characteristics were analysed in detail, and based on the results, a correlation for the volumetric local convective heat transfer coefficient was developed.

A numerical investigation of turbulent fluid flow and heat transfer in porous media was carried out by Yang et al. [25]. They considered a T-junction mixing where a flow is vertically discharged in a three-dimensional fully developed channel flow. The governing equations were also solved at the pore level using a turbulence model. An inline and a staggered arrangement of pores were investigated over a wide range of Reynolds numbers similar to that of Gamrat et al. [23]. Gaseous nitrogen with a uniform free stream velocity and a constant temperature entered a clear channel with a square cross-section. Similarly, nitrogen gases with uniform velocity and constant temperature (higher or lower than the channel inlet) were injected through the porous structure and mixed with the channel flow in a T-junction arrangement. The surfaces of the solid porous structure were kept at a constant temperature, equal to the channel flow whereas all other walls in the model were considered adiabatic. Heat transfer examination of the flow domain revealed that the temperature distribution in the porous structure was more uniform for the staggered array. Yang et al. [25] further found that the average Nusselt number in the porous medium increased drastically with increasing Reynolds number in the flow under an in-line array, while for the staggered array, it remained insensitive to Reynolds number.

Kim and Ghiaasiaan [35] modelled two-dimensional laminar, steady and pulsating flow through porous media. Their investigated system included several unit cells of porous structures with sinusoidal temporal variations in inlet flow. The porous media consisted of periodic arrays of square cylinders with the porosity ranging from 0.64–0.84. The Navier-Stokes equations were solved for pore-level simulations (microscopic equations) and the obtained results were compared with the volume-averaged equations (macroscopic equations) such as the Darcy-Forchheimer momentum equation. The Reynolds number, based on the unit cell length, of 0.1–1000 was set for steady flow while, that based on the mean superficial velocity (0.11 and 560) was used for unsteady simulations. The oscillatory flow consisted of pulsating frequencies ranging between 20–64 Hz with a fixed amplitude of 0.4 for all cases. Kim and Ghiaasiaan [35] stated that although the inlet velocity was sinusoidal, the calculated velocity was not exactly sinusoidal, indicating the existence of a non-linearity in the behaviour of the system. They concluded that the application of the Darcy-extended Forchheimer momentum equation with coefficients representing steady flow to pulsating flow conditions is only adequate at very low-flow (low frequency) conditions [35].

Alshare et al. [36] computed laminar steady and unsteady fluid flows and heat transfer for a spatially periodic array of square rods representing two-dimensional isotropic and anisotropic porous media. Uniform heat flux boundary conditions were imposed on the solid-fluid interface where the Reynolds number was varied between 1 and 1000. The microscopic details of the rod arrangement and flow angularity were used to determine the effective anisotropic properties of the porous medium. The flow was varied from 0–90° relative to the unit cell where the working fluid was air. Alshare et al. [36] argued that the permeability of the isotropic medium was uniform and independent of the flow angle, while for the anisotropic medium, the permeability varied nearly linearly between the two principal permeabilities.

Using the same geometry as Kim and Ghiaasiaan [35], Pathak and Ghiaasiaan [37] investigated solid-fluid heat transfer and thermal dispersion in laminar pulsating flow through porous media. Two dimensional, laminar flows in porous media were composed of periodically configured arrays of square cylinders with sinusoidal temporal disturbances on the inlet flow. Detailed numerical data was obtained for porosities of 0.64–0.84, frequencies of 0–100 Hz, and Reynolds numbers of 70–980. Pore-scale volume-averaged heat transfer coefficients and the thermal dispersion term were found to be strong functions of porosity, Reynolds number, and most importantly, the flow pulsation frequency. Based on the obtained numerical data, correlations were developed for the cycle-averaged, pore-scale Nusselt number and the dimensional thermal dispersion term. Pathak et al. [38] presented a numerical investigation of the hydrodynamics and conjugate heat transfer in porous media with unidirectional-steady and oscillatory flows. The pore-scale simulations used helium as the inlet fluid with steady and oscillatory flow at two amplitudes and frequencies between 0–60 Hz. The obtained data was then used to calculate numerous parameters including the unit-cell-length-based Nusselt number. It was concluded that predictive methods and correlations based on unidirectional steady flow should be avoided in the analysis of periodic flow systems in porous media.

Penha et al. [22] developed a transport model subject to periodic boundary conditions that describe incompressible fluid flow through a uniformly heated porous solid. The transport model used a pair of pore scale energy equations to define conjugate heat transfer. To cope with the geometrically complex domains, Penha et al. [22] developed a numerical method for solving the transport equations on a Cartesian grid. The results obtained by Penha et al. [22] corresponded to two structured models of porous media: an inline and a staggered arrangement of square rods on fully developed flows with isothermal walls. The approximation was modelled as a three-dimensional array with a REV where the Reynolds number was defined with respect to the reference length of the model, as was the Nusselt number. The effects of various system parameters on the Nusselt number were studied for both arrangements of square rods. Reasonable agreement was shown with the results of Kuwahara et al. [31] and other studies for Reynolds number $\geq$ 10 with the inline arrangement and for the staggered arrangement, while the two models were almost identical for 10 $<$ Reynolds number $\leq$ 100.

It follows from the review of literature that the existing pore-scale studies on unsteady heat convection in porous media are chiefly concerned with the accurate evaluation of Nusselt number. Unsurprisingly, this demands conduction of rather extensive computations which are often highly expensive and time consuming. However, a number of evolving technologies [9,12] require prediction of heat transfer rates in short durations with limited computational power and under highly dynamic conditions. Hence, there is a pressing need for the development of low-cost predictive tools to evaluate the dynamic response of heat transfer in porous media. Yet, as of now, there exists almost no systematic study on such tools. The current work aims to address this issue by using the outcomes of a pore-scale computational model for the development of a predictive heat transfer tool introduced by the classical theory of control. The study further determines the applicability range of the developed tool through evaluating the non-linearity of the dynamic response of heat convection in porous media.

The rest of this paper is organised as follows. First, the theoretical and numerical methods utilised by the investigation is presented. This is followed by a discussion of the results and a summary of the key findings and conclusions of the work.

2. Methodology

Determining the heat transfer characteristics inside porous media can be a cumbersome task [39]. Unsteady, multi-dimensional, pore-scale, simulations are necessary to understand the complex transport and the thermal dynamic response of these systems [40].

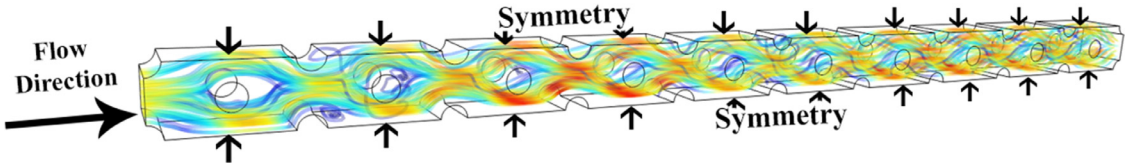

Fig. 1. General sketch of the 3-D pore scale model.

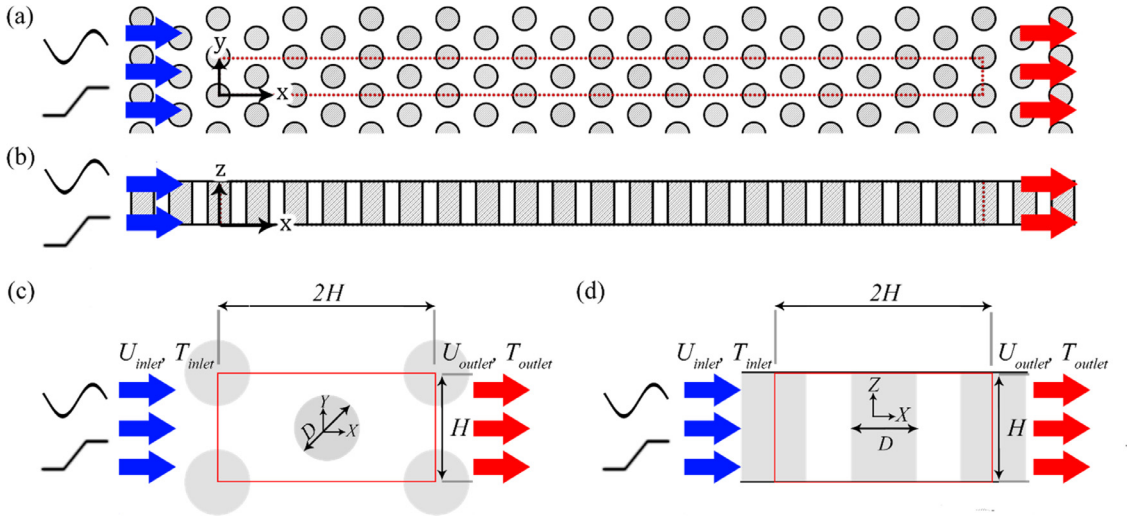

Fig. 2. Physical model and the coordinate system (a) coordinate system in x-y plane (b) coordinate system in x-z plane (c) single pore structural unit with boundaries in x-y plane (d) single pore structural unit with boundaries in x-z plane.

2.1. Problem configuration

A general sketch of the system modelled in this investigation is shown in Fig. 1 and a schematic diagram is shown in Fig. 2. A porous medium is represented by a series of staggered cylinders over which the fluid flows. The working fluid enters the domain through a uniform flow moving from left to right. The computational domain has a total length, l, height, H, while $l / H = 20$ and a flow obstacle (cylinder) diameter, D, for which $D/ H = 0.4$. The base configuration has a porosity, ε, of 0.874. However, the porosity of the porous structures changes with the cylinder diameter. The working fluids are air, hydrogen and carbon dioxide.

Ten cylinders are employed along the x-axis. Extensive numerical tests revealed that increasing the number of cylinders beyond this number does not change the statistics of the flow, and thus the flow at the end of the current computational domain can be deemed fully developed.

To determine the minimum required number of flow obstacles, simulations were performed on a unit cell model (based on Saito and de Lemos [41] approach) with periodic boundary conditions at the inlet and outlet with an obstacle diameter of 0.05 m. The solid walls were set to isothermal boundary conditions with a temperature of 300 K where no slip conditions were imposed. The inlet temperature was set to 200 K assuming uniform fluid flow. Although the unit cell model is representative of the inner element in a porous medium, its application is restricted to steady state conditions. As a result, a carefully devised approach was taken to generate a numerical model suitable for unsteady simulations. This involved utilising the steady unit cell model as a foundation and then generating a script to re-insert the velocity and temperature profiles from the outlet to the inlet. These simulations were run continuously until the variance between the inlet and outlet fell below a designated threshold, described by the Relative Profile Change, $RPC = \left(\sum_{profile} \frac{|\psi_{outlet} - \psi_{inlet}|}{\psi_{outlet}} \right) \times 100$ in which ψ is either the velocity or temperature. Table 1 displays the results of this study for three different values of the Reynolds number. Evidently, after approximately 9 iterations and for all Reynolds numbers the change in RPC falls below 5%. Hence, it was decided to model the REV using ten identical obstacles. For validation, the new model was investigated with the exact same conditions as the unit cell model. The tests showed the pressure and temperature profiles to be almost identical to the profiles after nine level of injections. Thus, a ten obstacle configuration (as shown in Figs. 1 and 2) was selected to carry out the investigations reported in the rest of this paper.

Table 1
Relative Profile Change Vs *Re*-injection iteration at different Reynolds numbers.

	Relative Profile Change%		
Injection Level (-)	Re_L=50	Re_L=200	Re_L=300
1	75.6	93.6	90
2	27.6	58.3	58.4
3	10.1	36.9	40.6
4	3.8	23.6	28.6
5	1.3	15.2	19.9
6	0.6	9.5	14.1
7	0	6.1	9.9
8	0	4	7.1
9	0	2.6	5
10	0	1.4	3.4
11	0	1.1	2.1
12	0	0.5	1.8

Steady state and unsteady responses are considered for the operation of the pore-scale model. This study focuses on the thermal dynamic response at the pore level, with the introduction of sinusoidal disturbances on the velocity fluctuations at the inlet (see Figs. 2a, 2b and 2c). Two symmetry planes are imprinted above

and below the working model along the *y*-axis to reduce the computational costs and time.

The numerical simulations were conducted using STAR-CCM+ 12.04.010 – a finite volume based Computational Fluid Dynamics software. An unsteady, three-dimensional, laminar flow model, coupled with the energy equation, was implemented within the fluid region for higher stability.

The following assumptions are made throughout the current analysis.

- The flow is laminar. This is justified by noting that the Reynolds numbers used in this study remain always below 325.
- The boundary conditions are time independent, and temporal oscillations are imposed on the inlet flow.
- As shown in Figs. 1 and 2, an unconsolidated porous medium is considered.

2.2. Governing equations, boundary conditions and numerical flow solver

The conservation of mass for the fluid flow between the inlet and outlet is given by

$$\frac{\partial \rho}{\partial t}+\frac{\partial(\rho u_x)}{\partial x}+\frac{\partial(\rho u_y)}{\partial y}+\frac{\partial(\rho u_z)}{\partial z}=0, \tag{1}$$

as the mass flux enters and leaves the model. Conservation of momentum for the fluid flow through the pores in x, y and z directions read

$$\begin{aligned}\rho\left(\frac{\partial u_x}{\partial t}+u_x\frac{\partial u_x}{\partial x}+u_y\frac{\partial u_x}{\partial y}+u_z\frac{\partial u_x}{\partial z}\right)=&\\ -\frac{\partial p}{\partial x}-\frac{\partial}{\partial x}\left[-2\mu\frac{\partial u_x}{\partial x}+\frac{2}{3}\mu\left(\frac{\partial u_x}{\partial x}+\frac{\partial u_y}{\partial y}+\frac{\partial u_z}{\partial z}\right)\right]&\\ -\frac{\partial}{\partial y}\left[-\mu\left(\frac{\partial u_x}{\partial y}+\frac{\partial u_y}{\partial x}\right)\right]-\frac{\partial}{\partial z}\left[-\mu\left(\frac{\partial u_x}{\partial z}+\frac{\partial u_z}{\partial x}\right)\right],&\end{aligned} \tag{2a}$$

$$\begin{aligned}\rho\left(\frac{\partial u_y}{\partial t}+u_x\frac{\partial u_y}{\partial x}+u_y\frac{\partial u_y}{\partial y}+u_z\frac{\partial u_y}{\partial z}\right)=&\\ -\frac{\partial p}{\partial y}-\frac{\partial}{\partial x}\left[-\mu\left(\frac{\partial u_x}{\partial y}+\frac{\partial u_y}{\partial x}\right)\right]&\\ -\frac{\partial}{\partial y}\left[-2\mu\frac{\partial u_y}{\partial y}+\frac{2}{3}\mu\left(\frac{\partial u_x}{\partial x}+\frac{\partial u_y}{\partial y}+\frac{\partial u_z}{\partial z}\right)\right]&\\ -\frac{\partial}{\partial z}\left[-\mu\left(\frac{\partial u_y}{\partial z}+\frac{\partial u_z}{\partial y}\right)\right],&\end{aligned} \tag{2b}$$

$$\begin{aligned}\rho\left(\frac{\partial u_z}{\partial t}+u_x\frac{\partial u_z}{\partial x}+u_y\frac{\partial u_z}{\partial y}+u_z\frac{\partial u_z}{\partial z}\right)=&\\ -\frac{\partial p}{\partial z}-\frac{\partial}{\partial x}\left[-\mu\left(\frac{\partial u_x}{\partial z}+\frac{\partial u_z}{\partial x}\right)\right]-\frac{\partial}{\partial y}\left[-\mu\left(\frac{\partial u_y}{\partial z}+\frac{\partial u_z}{\partial y}\right)\right]&\\ -\frac{\partial}{\partial z}\left[-2\mu\frac{\partial u_z}{\partial z}+\frac{2}{3}\mu\left(\frac{\partial u_x}{\partial x}+\frac{\partial u_y}{\partial y}+\frac{\partial u_z}{\partial z}\right)\right],&\end{aligned} \tag{2c}$$

The conservation of energy for the heat transferring flow is written as

$$\rho c_p\left(\frac{\partial T}{\partial t}+u_x\frac{\partial T}{\partial x}+u_y\frac{\partial T}{\partial y}+u_z\frac{\partial T}{\partial z}\right)=\frac{\partial}{\partial x}\left(k_f\frac{\partial T}{\partial x}\right)+\frac{\partial}{\partial y}\left(k_f\frac{\partial T}{\partial y}\right)+\frac{\partial}{\partial z}\left(k_f\frac{\partial T}{\partial z}\right), \tag{3}$$

where all symbols have been defined in the nomenclature.

The pertinent boundary conditions include the no-slip condition on the external surface of the cylindrical obstacles. Further, the top and bottom of the model in the y-direction are selected as the symmetry planes (Fig. 2a). The external surface of the ten obstacles of the model are all set to a constant temperature of 700 K. The outlet has an initial condition with the ambient temperature (300 K) and is under atmospheric pressure. A coupled flow solver was used to model the fluid flow, while steady and implicit unsteady solvers were used throughout this study.

Under steady conditions, the fluid flow at the inlet was modelled with a uniform velocity and an inlet temperature of 300 K. The inlet flow velocity was then modulated in time by superimposing a sinusoidal wave with variable amplitude and period (frequency):

$$u(0,t)=u_{in}\cdot(1+as\ in(2\pi\cdot f\cdot t)). \tag{4}$$

The Reynolds number based on the particle diameter is obtained by the following relation.

$$Re_L=\frac{u_{in}\rho D}{\mu}. \tag{5}$$

Within the pore-scale model, heat is transferred by forced convection as per Newton's law of cooling:

$$q_f''=h_o\left(T_f-T_{ref}\right). \tag{6}$$

The surface-averaged time-dependant Nusselt number was calculated over each obstacle of the porous structure to evaluate the thermal response of the system. The following relation was used to obtain the numerical value of the Nusselt number [23].

$$Nu_L=\frac{q_f''D}{k\left(T_f-T_{ref}\right)}. \tag{7}$$

A second-order discretization method was applied to all equations, and the converged solutions from the steady state simulations were used as the starting point for the unsteady simulations. The steady state simulations were performed for residual levels of 10^{-6} for all equations. The base time step was designated to be two orders of magnitude lower than the physical time scale, and a refined time step was implemented for unsteady cases to attain greater precision. Additionally, a considerably large value was set for the maximum time step in the unsteady cases. Furthermore, the average temperature at the outlet was observed to converge in time. If the simulations deviated in the final 1000-time steps by less than 0.5 K the simulations were set to be terminated.

A parametric study was subsequently conducted in which the Reynolds numbers, porosity, working fluids and frequency of the inlet velocity disturbances were varied systematically. Table 2 shows the operating conditions and the parameters of this study. It should be noted that the frequencies of the inlet disturbances are quite low ($f \leq 2$Hz). This is because only low flow velocities are considered in this work, and therefore the porous system will be slow in responding to temporal disturbances superimpose on the inlet flow.

2.3. Validation and grid independency

As shown in Fig. 3, a polyhedral staggered mesh was used with prism layers and finer spacing around the inlet, outlet and external surfaces of the obstacles. Computational tests were performed using a mesh with varying base size to determine the grid density that would achieve an adequate balance between computational power and accuracy. The base size specifies the reference length value for all relative size controls such as the surface size, maximum cell size, and total prism layer thickness. The value of base size varies depending on the model dimensions. To verify the grid independency of the numerical solution, the Nusselt number over

Table 2
Operating Conditions.

Other conditions							
Ambient temperature (K)	T_{amb}	300					
Frequency (Hz)	f	0.25	0.5	0.75	1	1.5	2
Reynolds Number	Re_L	50		150		250	
Geometry							
Pore scale model length (m)	l	2.0					
Particle diameter (cm)	D	4		5		6	
Porosity	ε	0.717		0.804		0.874	
Fluid		air		hydrogen		carbon dioxide	
Inlet temperature (K)	T_{in}	300					
Inlet pressure (MPa)	p_{in}	0.1					
Particle temperature (K)		700					

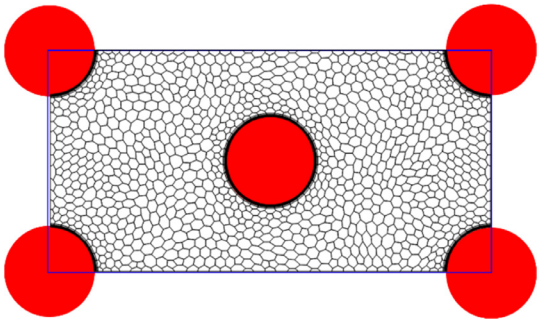

Fig. 3. Polyhedral staggered mesh of a single pore structural unit as implemented in the current simulations.

Table 3
Grid Independency.

	Cell Size (m)	Number of cells
Test 1	0.1	204,354
Test 2	0.05	543,607
Test 3	0.02	586,929
Test 4	0.01	611,772
Test 5	0.005	838,353
Test 6	0.003	1662,417
Test 7	0.001	15,662,124

the obstacles was investigated for seven different base sizes. This was performed with Re_L= 50 and ε = 0.717 and the outcomes are summarised in Table 3. As the mesh density is increased, the solution converges. The coarsest mesh, with a cell size of 0.1 m, fails to accurately capture the outlet temperature and Nusselt number on each particle. However, solutions obtained with grids consisting of hundreds of thousands of cells are reasonably accurate. Higher grid densities, up to a cell size of 0.001 m, yield no obvious advantage in accuracy. Hence, for the three-dimensional pore-scale model, all solutions presented in this work are achieved using a mesh with a cell size of 0.005 m. Precautions were taken to ensure sufficient mesh refinement, and adequate mesh resolution.

Table 4
Validation for Nusselt Number with Torabi et al. [20].

Re_D	Nu (ε = 0.717)	Nu (Torabi et al. [20])	% error
1	6.26	6.8	8.6
10	6.9	7	1.4
50	10.42	10.9	4.6
100	12.29	13	5.8
200	15.33	15.9	3.7

The current study is validated using the data reported in Ref. [20] with the use of a circular cross-section configuration, with varying Reynolds number. The Reynolds number and Nusselt number are calculated by using the Darcian velocity and the bulk temperature as the reference instead of the particle diameter. Table 4 shows good agreement between the current results and those of Ref. [20]. Further, Fig. 4 depicts favourable comparisons of the current results with the numerical data of Kawahara et al. [31] and Chen and Wung [42]. Furthermore, to evaluate the unsteady performance of the simulations, the current configuration without cylinders was exposed to different ramp disturbances in the flow

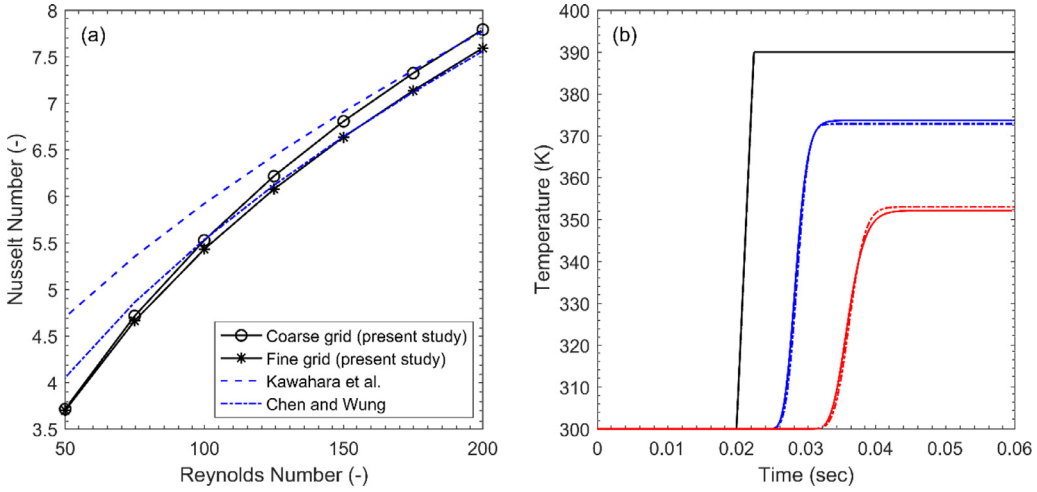

Fig. 4. a) Comparison between Nusselt Number calculated by the current simulation and those reported in Refs. [31,42] over a single obstacle; b) Temporal variations of temperature at inlet (black), centre (blue) and outlet (red) for unsteady response, solid and dash-dot lines represent DNS and the current simulations, respectively.

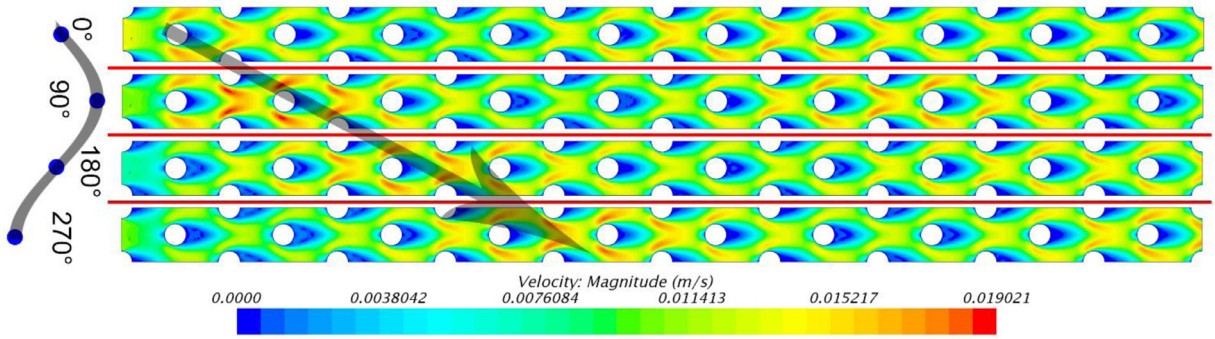

Fig. 5. Spatiotemporal evolution of the flow field exposed to a sinusoidal inlet velocity disturbance. Fluid type: CO_2, ?? = 0.874, Re_L=50, f = 0.25 Hz, a = 30%.

temperature. The predicted flow temperatures at different locations along the domain were compared to those predicted by direct numerical simulation (DNS) of the same problem [43]. The very good agreement observed in Figs. 4a and 4b confirms the validity of the current unsteady numerical simulations.

3. Results and discussion

Fig. 5 illustrates the spatiotemporal response of the investigated flow field to a sinusoidal velocity disturbance superimposed on the inlet flow. The figure corresponds to a case with high porosity and low Reynolds number in which the wake of each obstacle is shorter than the distance between two neighbouring obstacles. The steady flow includes low velocity wake regions behind the cylinders surrounded by relatively higher velocity regions formed by the passage of the flow between the cylindrical obstacles. As clearly shown in Fig. 5, modulation of the inlet flow by a sine wave results in a noticeable change in the magnitude of the velocity around the obstacles. This alteration in the flow velocity is advected by the mean flow and thus propagates downstream throughout the domain. Fig. 5 shows two advective sinusoidal disturbances. These include one shown on the left-hand side of the figures advecting through the first few pores of the systems (marked by an arrow), while the other disturbance has already proceeded towards the outlet. Clearly, influences of the disturbance upon the velocity field has decayed during the downstream propagation process. This is to be expected as the fluid viscosity tends to smear out the stronger velocity gradients induced by the flow disturbance. Modulations of the flow velocity alters the local heat convection coefficient, which in turn forms a temporal heat transfer response on the external surface of each obstacle. The dynamics of this response will be investigated in the later parts of this section.

Fig. 6 shows the temperature and velocity fields of an investigated porous medium exposed to sinusoidal disturbances at the inlet velocity. Development of the steady temperature field is shown in Fig. 6a. This represents a typical convective system with constant temperature boundaries in which the flow temperature approaches that of the boundaries towards the outlet. Introduction of a velocity disturbance does not appear to have any obvious effect

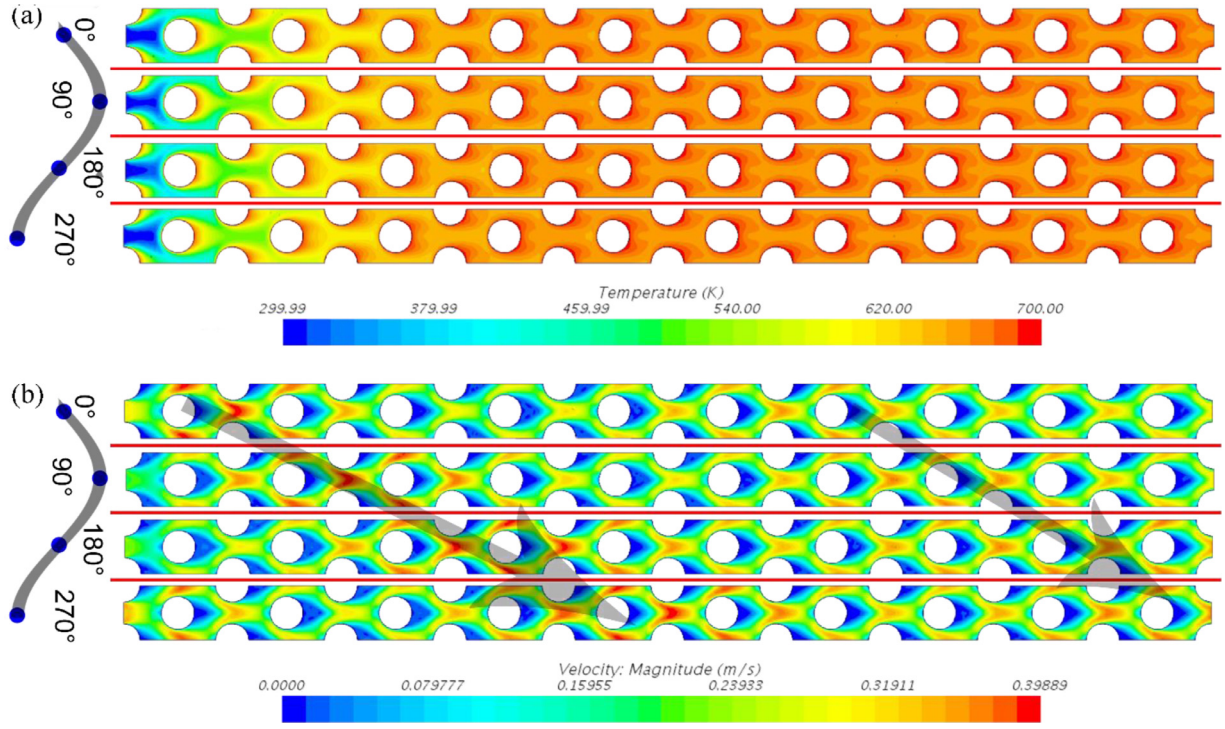

Fig. 6. Spatiotemporal evolution of the flow temperature and velocity fields exposed to a sinusoidal inlet velocity disturbance. Fluid type: H_2, ?? = 0.717, Re_L=50, f = 0.25 Hz, a = 30% (a) temperature field (b) velocity field.

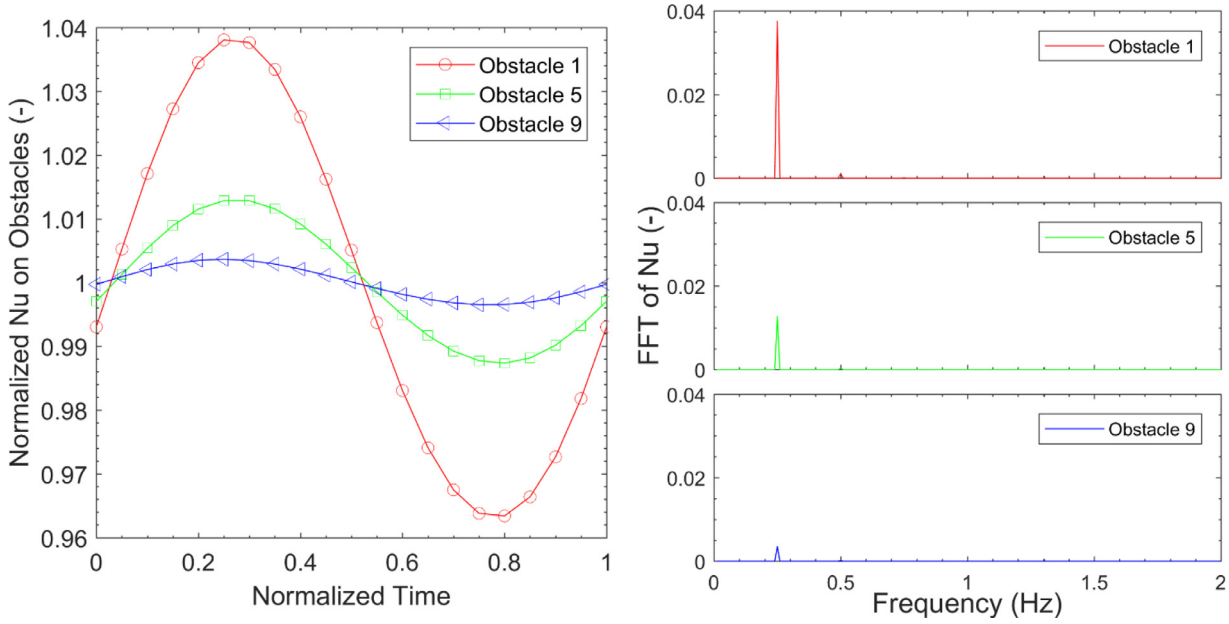

Fig. 7. (a) Temporal evolution of the normalised Nusselt number over three different obstacles (normalised time=time (s)/period of sine wave(s)), (b) Spectrum of Nusselt number. Fluid: air $\varepsilon = 0.874$ Re_L=50 $f = 0.25$ Hz.

upon the flow field. It will be shown later that this is because the velocity disturbance in this case induces a relatively small perturbation in the heat convection coefficient. Nonetheless, it will be argued that the heat transfer and subsequently the temperature fields are affected by the disturbance. Fig. 6b shows the spatiotemporal evolution of the flow field during a full period of inlet velocity modulation by a sine wave. The trends shown in this figure are qualitatively similar to those discussed in Fig. 5. However, the changes in the fluid type and the porosity of the medium have resulted in the intensification of the velocity effects of the flow disturbance. It is worth noting that the local maximum velocity in Figs. 6b and 5 are well below 1 m/s (Reynolds numbers below 325) and thus the transition to turbulence in any part of the flow remains unlikely.

The normalised Nusselt number on each obstacle is defined as $Normalised\ Nu = Nu_L \div \overline{Nu_L}$ where $\overline{Nu_L}$ is the mean Nusselt number averaged over the entire external surface area of the obstacle in the steady flow. Fig. 7 shows the time trace of the normalised Nusselt number when the flow is modulated by a sinusoidal disturbance with a frequency of 0.25 Hz. It is clear that the temporal response of the Nusselt number over the three examined obstacles closely resembles a sine wave, while there is a significant drop of the amplitude for those obstacles that are located farther from the inlet. This observation is further confirmed by the spectra of the traces of Nusselt numbers' response (calculated through using fast Fourier transform, FFT) shown in Fig. 7b. The occurrence of response at the same frequency as the input excitation is a classical sign of a linear system [44,45]. It is, therefore, inferred that in this case heat transfer in the porous medium can be approximated as a linear dynamic system.

The dynamics of a linear system can be readily predicted by a transfer function, which gives information on both the amplitude and phase of the response [44]. The transfer function of a linear dynamical system can help predict the responses of such a system to any input disturbance. This is because any arbitrary disturbance at the system input can be decomposed into a series of sinusoidal disturbances by utilising the Fourier transform. The transfer function enables predicting the system response to each of those sinusoids and the linearity of the system allows adding them to determine the system response to the arbitrary input disturbance. The concept of a transfer function is usually used for a single input, single output system. Here, we consider the oscillating inlet flow as the input of a dynamic system for which the oscillating normalised Nusselt number at a given obstacle is the output. As a result, in the current problem, ten transfer functions can be defined for the ten considered obstacles (see Fig. 2). The amplitude of these transfer functions is defined as $a(\omega) = |Normalised\ Nu_{Li}(\omega)|$ in which i denotes the obstacle number. The amplitude and phase of these transfer functions were calculated for all obstacles and two representative set of results are shown in Fig. 8. The amplitudes of the transfer functions shown in Figs. 8a and 8b clearly indicate that the system is most responsive to the lowest excitation frequencies. As expected, the amplitude of the response for the obstacles situated farther from the inlet is significantly smaller than those located upstream. This is due to the decay of disturbance throughout the advection process (see Figs. 5 and 6). As the frequency of the input sine wave increases, the amplitude of the response drops considerably. This behaviour can be consistently observed for all the obstacles considered in Figs. 8a and 8b. The strong response of the normalised Nusselt number to low-frequency sinusoids is in keeping with those already reported for other mechanical [46] and thermal systems [47,48]. In general, low-frequency disturbances provide a longer time for a physical system to respond and thus a larger amplitude is often obtained at low frequencies of the input disturbance. In the current case, the low-frequency sinusoidal disturbances provide enough time for the process of heat convection on the surface of the obstacle to be completed. Yet, as the frequency of the flow disturbance increases, the available time for the interactions between the disturbance and heat convection becomes shorter and thus the amplitude of the response diminishes. Although not shown in Fig. 8, a simple extrapolation reveals that at a certain high frequency, the system response drops to almost zero. This is where the disturbance is temporally so short that the heat convection process essentially cannot respond to it. Once again, this feature is analogous to those reported for other thermofluid systems [47,48].

Figs. 8c and 8d indicate that the phase of the transfer function resembles that of a classic convective lag [45]. This is the time

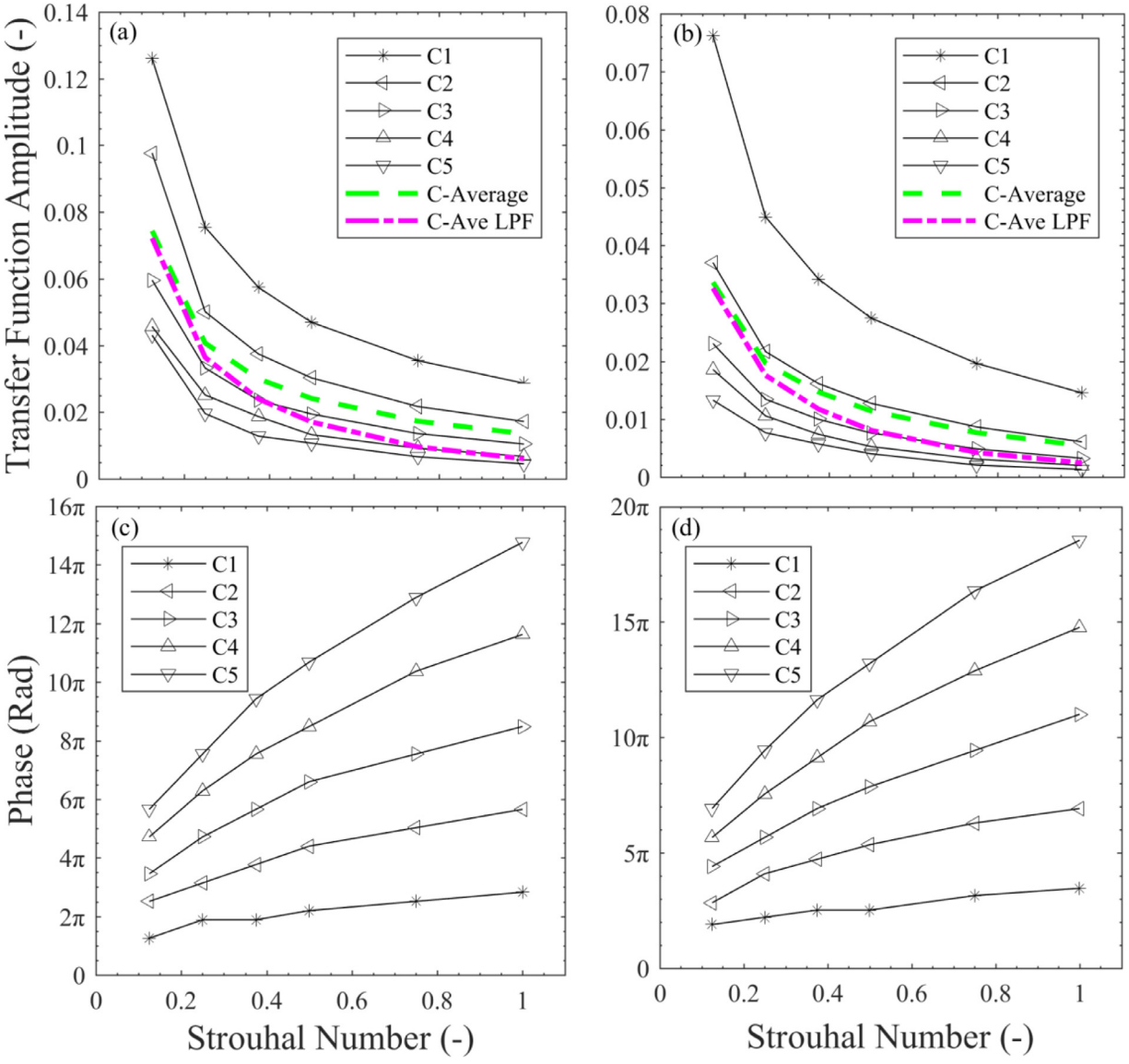

Fig. 8. Transfer functions of heat convection evaluated over different obstacles (C1-C5), (a) Fluid: CO_2, ?? = 0.874 Re_L =50– Transfer function amplitude, (b) Fluid: H_2, ?? = 0.804 Re_L =50– Transfer function amplitude, (c) Fluid: CO_2, ?? = 0.874 Re_L =50– Phase of transfer function, (d) Fluid: H_2, ?? = 0.804 Re_L =50– Phase of transfer function.

elapsed for the flow disturbance to move from the inlet to a given particle. For a system with a constant convective lag, the phase will be a straight line. The deviation from this implies changes in the advective velocity of the disturbance. As already discussed, this is because of the decay and annihilation of the initial disturbances during the process of advection over flow obstacles. Considering these trends, the transfer function of the thermal system including all ten obstacles can be approximated in two different ways. First, the responses of all obstacles can be simply averaged. Second, the amplitude of the thermal system can be approximated as a 'low-pass filter' [49,50,51] while, the phase is governed by a convective lag. It is well established that many thermofluid systems are practically low-pass filters [52,53]; as such they respond only to low frequencies and become irresponsive to any excitation that exceeds a certain frequency. The low-pass filter only allows low frequency signals from 0 Hz to a cut off frequency, f_c to pass whilst blocking those any higher. From visual inspection, it can be seen in Figs. 8a and 8b that the cut-off frequency is around a Strouhal number of one. Eqs. (8a) and (8b) are the modified relations used to create a low-pass filter for the average amplitude of the thermal system [52,53].

$$Low\ pass\ filter = \bar{a} \cdot \frac{X_C}{\sqrt{R^2 + X_C^2}}, \tag{8a}$$

$$X_C = \frac{1}{2\pi fC}, \tag{8b}$$

where all terms are defined in the nomenclature. The low-pass filter introduced in Eqs. (8a) and (8b) and illustrated in Fig. 8 represents an approximation of the heat transfer dynamics of the porous system. Fig. 8 further shows that the amplitude of the transfer function predicted by the low-pass filter is close to the average response. The phase of the system can be simply approximated by that of $e^{i2\pi f(t+\tau_j)}$ in which τ_j is the time taken for the disturbance to travel from the inlet to obstacle j.

The foregoing findings on the transfer function were entirely based upon the assumption of linearity of the system, as confirmed by Fig. 7. However, there are cases for which the system dynamics are no longer linear. For example, Fig. 9 shows the time trace and spectrum of the Nusselt number for a case similar to that shown in

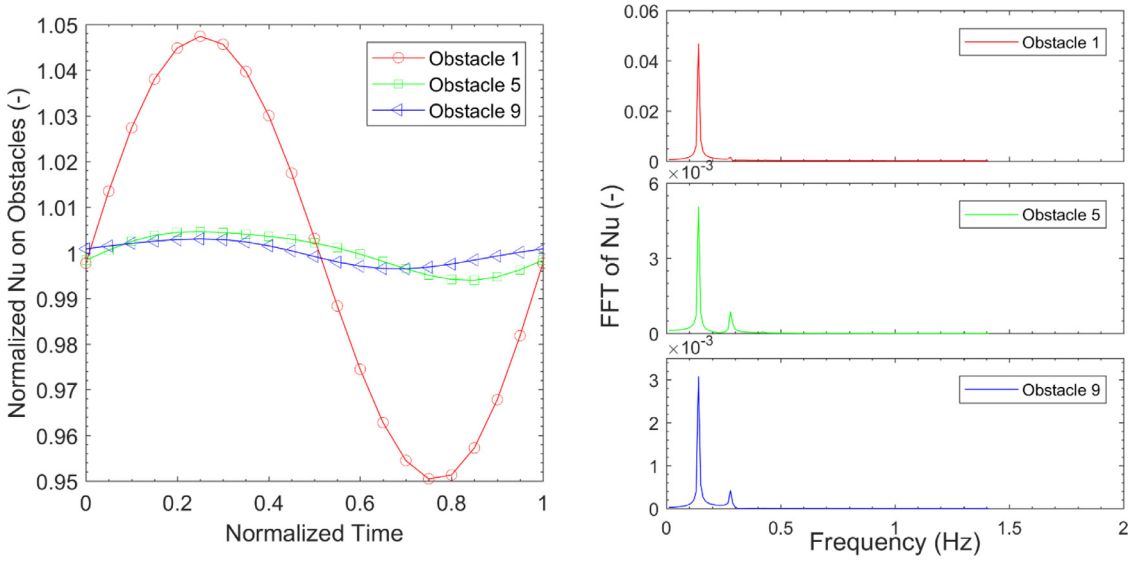

Fig. 9. (a) Temporal evolution of the normalised Nusselt number on three different obstacles (normalised time=time (s)/period of sine wave(s)), (b) Spectrum of Nusselt number. Fluid: CO_2 ?? = 0.804, Re_L =150, f = 0.25 Hz.

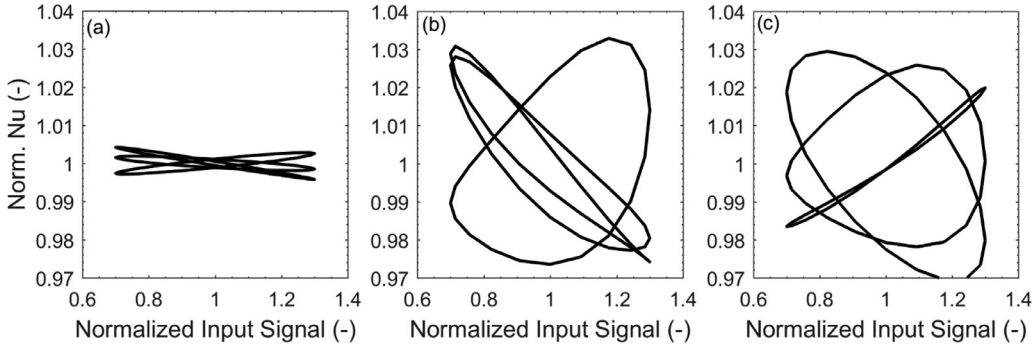

Fig. 10. Phase Portrait (Lissajous pattern), (a) linear case: Air, ?? = 0.804, Re_L =50, f = 0.25 Hz, (b) mildly non-linear case: Air, ?? = 0.804, Re_L =250, f = 0.25 Hz, (c) non-linear case: CO_2, ?? = 0.804, Re_L =250, f = 0.75 Hz.

Fig. 7 but with a different type of fluid and a higher Reynolds number. The appearance of two peaks in the spectra, particularly for obstacles farther from the inlet, is a clear indication of deviation from linearity. This is further supported by Fig. 10 which shows the phase portrait (Lissajous pattern) of the normalised Nusselt number calculated for three different cases. Fig. 10a corresponds to a case with a linear response in which the oval shapes in the phase portrait are axisymmetric. However, this feature disappears in Figs. 10b and 10c indicating a progressive departure from the linear response. Fig. 10c corresponds to a strongly nonlinear system for which the phase portrait can become significantly asymmetric [54]. Prediction of the dynamics of nonlinear systems is quite involved and, in many instances, the only way to predict the behaviour of such systems is through high-order modelling, which can be computationally expensive. This is, of course, very different from the linear approach discussed earlier in which the whole dynamics could be inferred from the transfer function with little computational cost. It is therefore essential to identify the conditions under which the system can be approximated as a linear system. This, in turn, calls for the quantification of nonlinearity.

Here, a measure of non-linearity is introduced to evaluate the deviation from linearity of the response. This is given by

$$\delta = \frac{n}{n-o}, \tag{9}$$

where δ is the measure of non-linearity, n, Euclidean norm of the normalized Nusselt number recorded at each obstacle and o is the discrete Fourier transform single-sided amplitude spectrum of the normalized Nusselt number at each obstacle [55] . Eq. (9) assigns a value of 0 to a completely linear system and gives a value of 1 to a completely nonlinear system. Thus, any real dynamic system will be assigned a value between 0 and 1. Fig. 11 shows the values of the measure of non-linearity (δ) calculated for all ten obstacles, indicating that the extent of nonlinearity can vary significantly with frequency. That is to say that for a given obstacle, the Nusselt number can respond almost linearly to a disturbance at one frequency and strongly nonlinearly to another frequency. Fig. 11 shows that the response of all obstacles to high frequency disturbances remains nearly linear. However, the response to the lowest frequency can be strongly nonlinear. The physical origin of nonlinearly in the present problem is the interactions between the flow disturbances and the boundary layers around the obstacles as well as those with the wake region behind the obstacle. Such interactions are very complex, and their predictions require detailed analysis. The current results indicate that the long duration (low frequency) disturbances have sufficient time to go through these interactions and thus can render a nonlinear response. However, the short-term high-frequency disturbances somehow by-pass the fluid dynamic interactions, providing an almost linear response with a smaller amplitude.

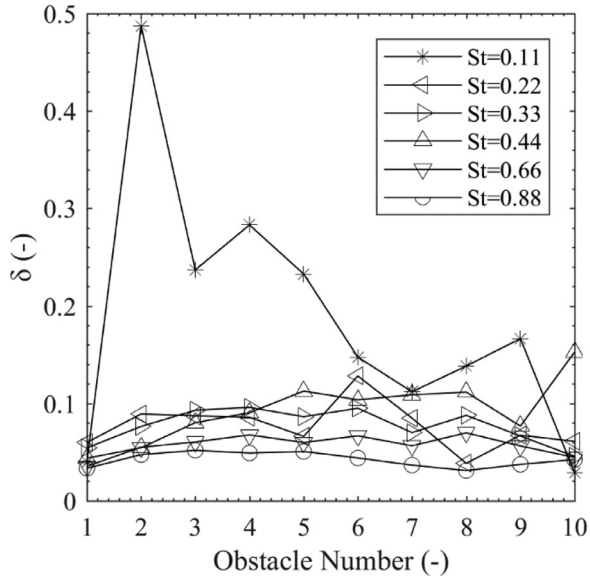

Fig. 11. The value of measure of nonlinearity of Nusselt Number over different obstacles – Fluid: Air, ?? = 0.874, Re_L =250.

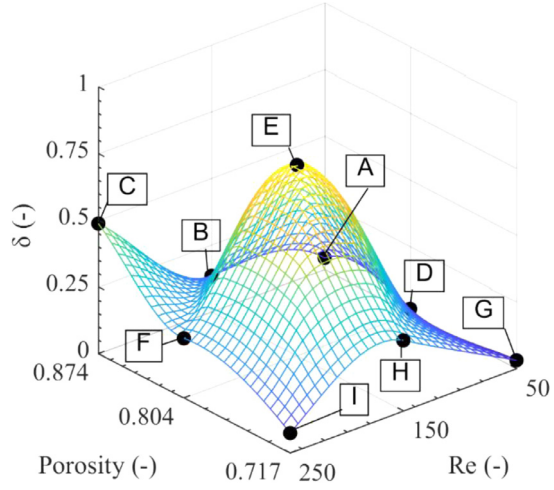

Fig. 12. The maximum value of measure of nonlinearity in Nusselt Numbers, for air. A) St=0.125, C9 B) St=0.125, C7 C) St=0.125, C2 D) St=0.125, C2 E) St=0.125, C8 F) St=0.125, C2 G) St=1, C2 H) St=0.125, C6 I) St=0.25, C2.

Here, the focus is on identifying the conditions for which the nonlinear response can be safely ignored and thus the dynamics of heat transfer can be predicted by the straightforward transfer function approach. Fig. 12 shows the maximum non-linearity factor as a function of porosity and Reynolds number for all six investigated Strouhal numbers and across all ten obstacles with the working fluid of air. This figure shows the maximum value of the measure of nonlinearity for each combination of Reynolds number and porosity (total of 9). It also specifies the obstacle number and Strouhal number for which the maximum is reached. This figure clearly shows that there is no monotonic trend with Reynolds number and porosity. For example, the maximum value of the measure of nonlinearity at Re_L=50 is close to zero and it increases to a higher value as the Reynolds number increases to 150. However, it drops down again when the Reynolds number increases to 250. This is an important result, as there is often a notion that lower Reynolds numbers render linear response and higher Reynolds numbers contribute to nonlinearity. Such an expectation stems from the macroscopic models of fluid flow in porous media (e.g. the Darcy and Darcy-Brinkmann-Forchheimer models) which add nonlinearity only to the higher Reynolds number flows. However, the current results indicate that for a dynamic problem the situation can be more complicated, and the Reynolds number and porosity can both affect the level of nonlinearity in a non-monotonic fashion. Fig. 12, nonetheless, shows that, regardless of the value of porosity, the level of nonlinearity always remains reasonably small at the lowest investigated Reynolds number (Re_L=50). It can be postulated that for low enough Reynolds numbers, the system is almost linear and thus the transfer function approach can be utilised to predict the dynamics of heat transfer. Yet, increases in Reynolds number do not necessarily push the system towards a nonlinear response.

4. Summary and conclusions

Unsteady forced convection in porous media can occur in systems subject to time-varying inlet flows. Examples of such systems can be readily found in electrochemical systems and porous burners used for the combustion of renewable fuels. In these applications, it is necessary to predict the heat transfer response of the system to arbitrary disturbances superimposed upon the inlet flow. Although it is possible to numerically model such responses, doing so is likely to be computationally demanding. Yet heat transfer predictions should be made over a short period of time with limited computational power. It is, therefore, desirable to use the classic methods of predicting the system dynamics without conducting a detailed computational study for every disturbance that the system may become exposed to. Nonetheless, such methods (e.g. transfer functions) are mostly limited to linear dynamical systems. This raises an important need to critically assess the linearity of the dynamic response of heat convection in porous media and to determine the conditions under which a transfer function approach can be used. To address this issue, a pore-scale analysis of unsteady forced convection was conducted in a reticulated porous medium consisting of several flow obstacles and subject to a temporally modulated inlet flow by a sinusoidal disturbance. The spatio-temporal evolutions of the flow disturbances within the investigated porous medium were simulated numerically. Furthermore, the Nusselt number on each flow obstacle was considered as the output of a dynamic system for which linearity was subsequently assessed. The key findings of this study can be summarised as follows.

- At low Reynolds numbers, the heat transfer response remains almost linear and therefore, a transfer function approach can be used to predict the system dynamics.
- The transfer functions of all obstacles are most responsive to low-frequency excitation and nearly insensitive to higher frequencies and, therefore closely resemble a low-pass filter.
- Low-frequency disturbances appeared to be more likely to lead to nonlinear response. This can be attributed to the availability of enough time for the flow disturbance to interact with the boundary layers formed around the obstacles.
- For linear cases, the average amplitude and phase response of the porous medium can be approximated by a low-pass filter and a convective lag, respectively.
- Calculation of the measure of nonlinearity revealed that, rather counterintuitively, increases in Reynolds number do not necessarily enhance the nonlinearity of the heat transfer response. In fact, non-monotonic trends in the level of nonlinearity were observed with respect to the Reynolds number and porosity of the medium.

It remains as a future task to develop low-cost models for prediction of the dynamics of heat transfer when the system is nonlinear.

Declaration of Competing Interest

The authors declare no conflict of interest

Acknowledgments

N. Karimi and B. Yadollahi acknowledge the finance support of Engineering and Physical Science Research Council through grant EP/N020472/1.

References

[1] Z. Kou, M. Dejam, Dispersion due to combined pressure-driven and electro-osmotic flows in a channel surrounded by a permeable porous medium, Phys. Fluids 31 (5) (2019) 056603.
[2] M. Dejam, Derivation of dispersion coefficient in an electro-osmotic flow of a viscoelastic fluid through a porous-walled microchannel, Chem. Eng. Sci. 204 (2019) 298–309.
[3] M. Dejam, Hydrodynamic dispersion due to a variety of flow velocity profiles in a porous-walled microfluidic channel, Int. J. Heat Mass Transf. 136 (2019) 87–98.
[4] M. Dejam, H. Hassanzadeh, Z. Chen, Shear dispersion in combined pressure–driven and electro-osmotic flows in a capillary tube with a porous wall, AIChE J 61 (11) (2015) 3981–3995.
[5] M. Dejam, H. Hassanzadeh, Z. Chen, Shear dispersion in combined pressure–driven and electro-osmotic flows in a channel with porous walls, Chem. Eng. Sci. 137 (2015) 205–215.
[6] Y. Deng, C. Feng, J. E, H. Zhu, J. Chen, M. Wen, H. Yin, Effects of different coolants and cooling strategies on the cooling performance of the power lithium ion battery system: a review, Appl. Therm. Eng. 142 (2018) 10–29.
[7] G. Xia, L. Cao, G. Bi, A review on battery thermal management in electric vehicle application, J. Power Sources 367 (2017) 90–105.
[8] J.L. Ellzey, E.L. Belmont, C.H. Smith, Heat recirculating reactors: fundamental research and applications, Prog. Energy Combust. Sci. 72 (2019) 32–58.
[9] Y. Mahmoudi, K. Hooman, K. Vafai, Convective Heat Transfer in Porous Media, CRC Press, 2019.
[10] G. Hunt, N. Karimi, B. Yadollahi, M. Torabi, The effects of exothermic catalytic reactions upon combined transport of heat and mass in porous microreactors, Int. J. Heat Mass Transf. 134 (2019) 1227–1249.
[11] G. Kolb, Review: microstructured reactors for distributed and renewable production of fuels and electrical energy, Chem. Eng. Process. Process Intensif. 65 (2013) 1–44.
[12] S. Wood, A.T. Harris, Porous burners for lean-burn applications, Prog. Energy Combust. Sci. 34 (5) (2008) 667–684.
[13] F. He, L. Ma, Thermal management of batteries employing active temperature control and reciprocating cooling flow, Int. J. Heat Mass Transf. 83 (2015) 164–172.
[14] H. Saberinejad, A. Keshavarz, M. Payandehdoost, M.R. Azmoodeh, A. Batooei, Numerical study of heat transfer performance in a pipe partially filled with non-uniform porous media under ltne condition, Int. J. Numer. Methods Heat Fluid Flow 28 (8) (2018) 1845–1865.
[15] Y. Mahmoudi, N. Karimi, "Numerical investigation of heat transfer enhancement in a pipe partially filled with a porous material under local thermal non-equilibrium condition, Int. J. Heat Mass Transf. 68 (2014) 161–173.
[16] F. Rong, W. Zhang, B. Shi, Z. Guo, "Numerical study of heat transfer enhancement in a pipe filled with porous media by axisymmetric tlb model based on gpu, Int. J. Heat Mass Transf. 70 (2014) 1040–1049.
[17] Y. Mahmoudi, N. Karimi, K. Mazaheri, Analytical investigation of heat transfer enhancement in a channel partially filled with a porous material under local thermal non-equilibrium condition: effects of different thermal boundary conditions at the porous-fluid interface, Int. J. Heat Mass Transf. 70 (2014) 875–891.
[18] C. Dickson, M. Torabi, N. Karimi, "First and second law analyses of nanofluid forced convection in a partially-filled porous channel – The effects of local thermal non-equilibrium and internal heat sources, Appl. Therm. Eng. 103 (2016) 459–480.
[19] X. Chu, G. Yang, S. Pandey, B. Weigand, "Direct numerical simulation of convective heat transfer in porous media, Int. J. Heat Mass Transf. 133 (2019) 11–20.
[20] M. Torabi, G.P. Peterson, M. Torabi, N. Karimi, A thermodynamic analysis of forced convection through porous media using pore scale modeling, Int. J. Heat Mass Transf. 99 (2016) 303–316.
[21] T. Ozgumus, M. Mobedi, "Effect of pore to throat size ratio on interfacial heat transfer coefficient of porous media, J. Heat Transfer 137 (1) (2014) 012602––9.
[22] D.J. Lopez Penha, S. Stolz, J.G.M. Kuerten, M. Nordlund, A.K. Kuczaj, B.J. Geurts, "Fully-developed conjugate heat transfer in porous media with uniform heating, Int. J. Heat Fluid Flow 38 (2012) 94–106.
[23] G. Gamrat, M. Favre-Marinet, S. Le Person, Numerical study of heat transfer over banks of rods in small reynolds number cross-flow, Int. J. Heat Mass Transf. 51 (3–4) (2008) 853–864.
[24] G. Hunt, N. Karimi, M. Torabi, "Two-dimensional analytical investigation of coupled heat and mass transfer and entropy generation in a porous, catalytic microreactor,", Int. J. Heat Mass Transf. 119 (2018) 372–391.
[25] G. Yang, B. Weigand, A. Terzis, K. Weishaupt, R. Helmig, "Numerical simulation of turbulent flow and heat transfer in a three-dimensional channel coupled with flow through porous structures, Transp. Porous Media 122 (1) (2018) 145–167.
[26] M. Dejam, H. Hassanzadeh, Z. Chen, Semi-analytical solution for pressure transient analysis of a hydraulically fractured vertical well in a bounded dual–porosity reservoir, J. Hydrol. 565 (2018) 289–301.
[27] M. Dejam, H. Hassanzadeh, "The role of natural fractures of finite double–porosity aquifers on diffusive leakage of brine during geological storage of CO2, Int. J. Greenh. Gas Control 78 (2018) 177–197.
[28] M. Dejam, H. Hassanzadeh, "Diffusive leakage of brine from aquifers during CO2 geological storage, Adv. Water Resour. 111 (2018) 36–57.
[29] M. Dejam, H. Hassanzadeh, Z. Chen, Pre-Darcy flow in porous media, Water Resour. Res. 53 (10) (2017) 8187–8210.
[30] M. Dejam, H. Hassanzadeh, Z. Chen, Semi-Analytical solutions for a partially penetrated well with wellbore storage and skin effects in a double-porosity system with a gas cap, Transp. Porous Media 100 (2) (2013) 159–192.
[31] F. Kuwahara, M. Shirota, A. Nakayama, A numerical study of interfacial convective heat transfer coefficient in two-energy equation model for convection in porous media, Int. J. Heat Mass Transf. 44 (6) (2001) 1153–1159.
[32] F.E. Teruel, L. Díaz, "Calculation of the interfacial heat transfer coefficient in porous media employing numerical simulations, Int. J. Heat Mass Transf. 60 (1) (2013) 406–412.
[33] N.F. Jouybari, M. Maerefat, M.E. Nimvari, A pore scale study on turbulent combustion in porous media, Heat Mass Transf. und Stoffuebertragung 52 (2) (2016) 269–280.
[34] Z. Wu, C. Caliot, G. Flamant, Z. Wang, Numerical simulation of convective heat transfer between air flow and ceramic foams to optimise volumetric solar air receiver performances, Int. J. Heat Mass Transf. 54 (7–8) (2011) 1527–1537.
[35] S.-.M. Kim, S.M. Ghiaasiaan, Numerical modeling of laminar pulsating flow in porous media, J. Fluids Eng. 131 (4) (2009) 041203––9.
[36] A.A. Alshare, P.J. Strykowski, T.W. Simon, Modeling of unsteady and steady fluid flow, heat transfer and dispersion in porous media using unit cell scale, Int. J. Heat Mass Transf. 53 (9–10) (2010) 2294–2310.
[37] M.G. Pathak, S.M. Ghiaasiaan, "Convective heat transfer and thermal dispersion during laminar pulsating flow in porous media, Int. J. Therm. Sci. 50 (4) (2011) 440–448.
[38] M.G. Pathak, T.I. Mulcahey, S.M. Ghiaasiaan, Conjugate heat transfer during oscillatory laminar flow in porous media, Int. J. Heat Mass Transf. 66 (2013) 23–30.
[39] J.R. Howell, M.J. Hall, J.L. Ellzey, Combustion of hydrocarbon fuels within porous inert media, Prog. Energy Combust. Sci. 22 (2) (1996) 121–145.
[40] J. Chen, L. Yan, W. Song, D. Xu, Effect of heat and mass transfer on the combustion stability in catalytic micro-combustors, Appl. Therm. Eng. 131 (2018) 750–765.
[41] M.B. Saito, M.J.S. de Lemos, A correlation for interfacial heat transfer coefficient for turbulent flow over an array of square rods, J. Heat Transfer 128 (5) (2006) 444.
[42] C.J. Chen, T.-S. Wung, Finite analytic solution of convective heat transfer for tube arrays in crossflow: part II—Heat transfer analysis, J. Heat Transfer 111 (3) (1989) 641–648.
[43] L. Christodoulou, N. Karimi, A. Cammarano, M. Paul, S. Navarro-Martinez, State prediction of an entropy wave advecting through a turbulent channel flow, J. Fluid Mech. 882 (2020) A8.
[44] K. Ogata, Y. Yang, Modern Control Engineering, Volume 17, Pearson, NJ, Upper Saddle River, 2010.
[45] K. Ogata, System Dynamics, Volume 3, Prentice Hall, Upper Saddle River, NJ, 1998.
[46] N. Luhmann, Introduction to Systems Theory, 2013.
[47] K.R. McManus, T. Poinsot, S.M. Candel, A review of active control of combustion instabilities, Prog. Energy Combust. Sci. 19 (1) (1993) 1–29.
[48] N. Karimi, Response of a conical, laminar premixed flame to low amplitude acoustic forcing - A comparison between experiment and kinematic theories, Energy 78 (2014) 490–500.
[49] M. Gopal, I.J. Nagrath, Control Systems Engineering, 5th Editio., Anshan Ltd, 2009.
[50] A. Banerjee, Automated Electronic Filter Design, Springer International Publishing, Cham, 2018.
[51] A. Izadian, Fundamentals of Modern Electric Circuit Analysis and Filter Synthesis, Springer International Publishing, Cham, 2019.
[52] S. Candel, Combustion dynamics and control: progress and challenges, Proc. Combust. Inst. 29 (1) (2002) 1–28.
[53] T.C. Lieuwen, Unsteady Combustor Physics, Cambridge University Press, Cambridge, 2012.
[54] H.S. Strogatz, Nonlinear Dynamics and Chaos: With Applications to Physics, Biology, Chemistry, and Engineering, Second Edition, 2nd Editio., CRC Press, 2015.
[55] W.H. Moase, M.J. Brear, C. Manzie, The forced response of choked nozzles and supersonic diffusers, J. Fluid Mech. 585 (2007) 281–304.